

# Gradient Boosting Mapping for Dimensionality Reduction and Feature Extraction

Anri Patron, Ayush Prasad, Hoang Phuc Hau Luu, and Kai Puolamäki

University of Helsinki, Helsinki, Finland  
firstname.lastname@helsinki.fi

**Abstract.** A fundamental problem in supervised learning is to find a *good set of features* or *distance measures*. If the new set of features is of lower dimensionality and can be obtained by a simple transformation of the original data, they can make the model understandable, reduce overfitting, and even help to detect distribution drift. We propose a supervised dimensionality reduction method *Gradient Boosting Mapping* (GBMAP), where the outputs of weak learners—defined as one-layer perceptrons—define the embedding. We show that the embedding coordinates provide better features for the supervised learning task, making simple linear models competitive with the state-of-the-art regressors and classifiers. We also use the embedding to find a principled distance measure between points. The features and distance measures automatically ignore directions irrelevant to the supervised learning task. We also show that we can reliably detect out-of-distribution data points with potentially large regression or classification errors. GBMAP is fast and works in seconds for dataset of million data points or hundreds of features. As a bonus, GBMAP provides a regression and classification performance comparable to the state-of-the-art supervised learning methods.

**Keywords:** dimensionality reduction · supervised learning · boosting · concept drift.

## 1 Introduction

In supervised learning, the fundamental task is to learn a regressor or classifier function from a set of features—or distances between the training data points—to the target variable, a real number for regression or a discrete value for classification. Several algorithms for finding such regression/classifier functions have been developed [13,6], and the field is already quite mature, at least for “classical” regression and classification datasets with up to thousands of features. It has even been argued the improvements in supervised learning technology during the past decades have been marginal at best, and much of the progress has been illusory in the sense that, in real-world applications, the marginal gains may be swamped by other sources of uncertainty, such as concept drift, not considered in the classical supervised learning paradigm [12].

However, if the data features are selected carefully, even a simple model—such as linear or logistic regression—may perform competitively to the state-of-the-art supervised learning models. The simple model can be more understandable if the new features are obtained by a relatively simple transformation from the original data. Indeed, well-performing supervised learning models are often *black boxes* whose working principles are difficult or impossible to understand, which is problematic in many practical applications [10].

While there are established methods to estimate the regression or classification errors for data from the same distribution used in the training, there are fewer ways to do so for out-of-distribution data in the presence of *concept drift* [9]. In other words, it is difficult to estimate the *uncertainty of the predictions*, which again, for obvious reasons, may hinder the usability of the supervised learning models in real-world applications where we do not have the ground truth target variables available.

Our intuition is that in real-world regression or classification problems, only a subset of *local directions* in the feature space is relevant for the regression or classification task. We call a direction relevant if it affects the regressor/classifier output. A good feature or distance measure should depend only on the relevant directions in the feature space, and they should be insensitive, e.g., to random nuisance features. We postulate that such features are better than the original features for the supervised learning task and may allow the use of simpler models with competitive performance. Also, to detect prediction uncertainty due to concept drift, we postulate that only the distances to these relevant directions must be considered.

To this end, we introduce *Gradient Boosting Mapping* (GBMAP), a supervised dimensional reduction method based on the gradient-boosting idea that a complicated function can be learned by a sequence of simpler functions known as weak learners. The weak learners are incorporated sequentially so that at each step, the current weak learner tries to correct the errors (residuals) made by the model learned during the earlier steps. In gradient boosting, the family of weak learners should be specified in advance (possibly with some parameterized form) to pick out the best weak learner using an optimization procedure. The weak learners should have low variance and high bias, meaning that the model family of the weak learners should be sufficiently simple. The boosting procedure then aggregates these simple weak learners to create a strong learner who can capture a highly complicated supervised learning model while being robust enough to avoid overfitting. The most common family of weak learners is decision trees, where the corresponding gradient boosting scheme is eXtreme Gradient Boosting (XGBOOST) [3], providing piece-wise constant weak learners that converge to a constant value outside the training data distribution. As a side product of the boosting formulation, GBMAP can also be used as a regression/classification model whose performance is competitive with state-of-the-art models such as XGBOOST.

*Contributions* of this paper are: (i) we define a boosting-based embedding method GBMAP and show its theoretical properties (Sect. 3), (ii) we show the

embedding is fast to compute (e.g., the runtime on a dataset with a million data points of a dimension of 25 is around 15 seconds (Sect. 4.2), and that it performs comparatively to the state-of-the-art regression/classification models (Sect. 4.3) although regression/classification performance is not our primitive objective, (iii) show that the embedding features and the induced distance can be used as features for classification/regression (Sect. 4.4), and that (iv) GBMAP can detect outlier data points with potentially large regression/classification errors without seeing the ground truth target values (Sect. 4.5). Finally, we conclude the paper with a discussion of potential other applications for GBMAP (Sect. 5) and a future outlook (Sect. 6). We included supplementary material in the appendix that is not necessary to understand the contributions of the paper but gives, e.g., additional experimental results that complement those in the paper (Sects. A–F).

## 2 Related Work

The standard methods for dimensionality reduction/data visualization in machine learning are unsupervised methods such as Principal Component Analysis (PCA) [38] or t-distributed Stochastic Neighbor Embedding (t-sne) [20] that do not consider the target variable at all; the advantage is simplicity and that these methods can also be used for unlabeled data, but the obvious drawback is that if most features are irrelevant for the supervised learning task, the embedding may not be helpful. For this reason, supervised methods try to take the target variable into account. These methods include Linear Optimal Low rank projection (LOL) [35] and IVIS [33]. LOL works by calculating the mean of each class and the difference between these means. It then computes the class-centered covariance matrix, using the top eigenvectors and the mean difference to construct the embeddings. IVIS is a parametric method that uses a Siamese neural network architecture with a triplet loss function to preserve distances of data points in the embedding space.

The term *concept drift* means phenomena where the data distribution changes over time; for surveys, see [9,39,19]. Most concept drift detection methods need access to the ground truth target variables, especially those of test data points. However, in some real-world applications, we can only have access to the training labels, while the test labels are missing [22], and we have to evaluate drift based solely on the model prediction, training labels, and the covariate structures. Methods that detect drift merely based on covariate distribution shifts [32,26] suffer from irrelevant features, resulting in a high false alarm rate [31]. Therefore, taking into account the target variable (training labels, model prediction) is highly important. The literature is limited in this line of work and primarily focuses on concept drift in classification [31,18]. Recently, [22] proposed a drift detection algorithm for *time series* regression problems. In this work, we demonstrate an added benefit of GBMAP that its embedding distance can be used internally for drift detection, with high reliability for regression and classification tasks. It is worth noting that this is an efficient built-in concept

drift detection of GBMAP, eliminating the need for an external package to detect drift in GBMAP.

For the boosting literature, we refer to a textbook such as [13], where we have borrowed the notation used in this paper. Our ideas are mostly related to gradient boosting, where at each boosting iteration, the weak learner is updated to minimize the loss induced by the current strong learner [8], which is the accumulation of all previous weak learners. This work uses a family of perceptrons as weak learners to extract simple softplus-like functions from a complicated target function sequentially. These simple functions serve as interpretable feature extractors, as explained in Sect. 5.2. A related method is XGBOOST [3], which uses tree-based regressors and classifiers as weak learners; see Sect. 3.6 for a more detailed discussion.

### 3 Theory and Methodology

#### 3.1 Definition of Our Model

Assume we have  $n$  *training data* points  $(\mathbf{x}_1, y_1), \dots, (\mathbf{x}_n, y_n)$  drawn independently from a fixed but usually unknown distribution  $(\mathbf{x}_i, y_i) \sim F$ , where the target variable is  $y_i \in \mathbb{R}$  for regression,  $y_i \in \{-1, +1\}$  for binary classification, the covariate is  $\mathbf{x}_i \in \mathbb{R}^p$ , and  $i \in [n] = \{1, \dots, n\}$ .  $\mathbf{X} \in \mathbb{R}^{n \times p}$  denotes the data matrix where the rows correspond to observations,  $\mathbf{X}_{i \cdot} = \mathbf{x}_i^\top$ . In this work, we want to predict the value of  $y$  given  $\mathbf{x}$  by fitting a model  $f : \mathbb{R}^p \rightarrow \mathbb{R}$  to the training data. For regression problems, the prediction  $\hat{y}$  is then given directly by  $f$  as  $\hat{y} = f(\mathbf{x})$ . For classification problems, the probability of  $+1$  is given by  $\hat{p}(y = +1 | \mathbf{x}) = \sigma(f(\mathbf{x}))$ , where  $\sigma(z) = 1/(1 + e^{-z})$  is the sigmoid function (see Sect. A), and the predicted class by the sign as  $\hat{y} = \text{sign}(f(\mathbf{x}))$ .

We define  $f$  to be an ensemble of  $m$  weak learners  $f_j : \mathbb{R}^p \rightarrow \mathbb{R}$ , where  $j \in [m]$ , and an initial model  $f_0(\mathbf{x})$ , which be any function; we use by default  $f_0(\mathbf{x}) = 0$ . Other choices of  $f_0$  are possible depending on the application, as discussed in Sect. 5.1.  $f$  is given by

$$f(\mathbf{x}) = \sum_{j=0}^m f_j(\mathbf{x}). \quad (1)$$

Here—even though we end up with well-performing regressors and classifiers—our main motivation is not to make the best regressor or classifier but instead use the weak learners to find a lower-dimensional embedding. For this reason, we define the weak learners to be linear projections with non-linearity,

$$f_j(\mathbf{x}) = a_j + b_j g(\mathbf{w}_j^\top \mathbf{x}), \quad (2)$$

where the intercept and slope terms  $a_j \in \mathbb{R}$ ,  $b_j \in \{-1, +1\}$ , and the projection vectors  $\mathbf{w}_j \in \mathbb{R}^p$  are learned from data, as described later in Sect. 3.2. We assume that  $\mathbf{x}$  contains an intercept term (a feature which equals unity) if necessary. The nonlinearity is given by the function  $g : \mathbb{R} \rightarrow \mathbb{R}$ . In this work, we use softplus

$g_{soft+}^\beta(z) = \log(1 + e^{\beta z}) / \beta$ , the smooth variant (for more efficient optimization) of the ReLU  $\lim_{\beta \rightarrow \infty} g_{soft+}^\beta(z) = \max(0, z)$ .

Formally, we want to find  $f$  such that the generalization error defined by  $L = E_{(\mathbf{x}, y) \sim F} [l(y, f(\mathbf{x}))]$  is minimized, where  $l : \mathbb{R} \times \mathbb{R} \rightarrow \mathbb{R}_{\geq 0}$  is a predefined loss function. We use the quadratic loss  $l_{quadratic}(y, y') = (y - y')^2$  for regression problems and logistic loss  $l_{logistic}(y, y') = \log(1 + e^{-yy'})$  for classification problems. The logistic loss (used by logistic regression) can be viewed as a smooth variant (again, for easier optimization) of the hinge loss  $l_{hinge}(y, y') = \max(0, 1 - yy')$  (used, e.g., by support vector classifiers).

### 3.2 Learning the Model Parameters

The problem can be cast into  $2^m$  continuous non-convex optimization problems ( $2^m$  possibilities of  $b_j$ 's), which is NP-hard. The boosting scheme offers a greedy stage-wise search approach to explore this combinatorial state space. We can also view Eq. (1) as a discretized ensemble of  $m$  weak learners, 1-layer perceptrons.

Given the initial model  $f_0$  (by default,  $f_0(\mathbf{x}) = 0$ ), loss function  $l$ , non-linearity  $g$ , and the training data, we can use the boosting ideas to find our model's parameters  $a_j$ ,  $b_j$ , and  $\mathbf{w}_j$ . The boosting consists of  $m$  iterations. At  $j$ th iteration, we find the model parameters by solving the following optimization problem:

$$a_j, b_j, \mathbf{w}_j = \arg \min_{a_j, b_j, \mathbf{w}_j} (\mathcal{L}_j + \mathcal{R}_j), \quad (3)$$

where the empirical loss is

$$\mathcal{L}_j = n^{-1} \sum_{i=1}^n l \left( y_i, \sum_{k=0}^j f_k(\mathbf{x}_i) \right). \quad (4)$$

Recall that  $f_j(\mathbf{x})$  is parameterized by  $a_j$ ,  $b_j$ , and  $\mathbf{w}_j$ . Here, we use a Ridge regularization for numerical stability, given by  $\mathcal{R}_j = \lambda \sum_{k=1}^p \mathbf{w}_{jk}^2 / p$ . We use the limited-memory Broyden–Fletcher–Goldfarb–Shanno algorithm (LBFGS) implementation in Python JAXOPT library [2] to solve the optimization task in Eq. (3) for  $b_j = -1$  and  $b_j = +1$  separately, choosing the value of  $b_j$  that leads to the smallest loss. We find all of the functions  $f_j$  by repeating the optimization of Eq. (3) for all values of  $j$  starting from 1 and ending in  $m$ .

### 3.3 Embedding of Data Points

The most interesting advantage of our proposed method is that it can be used for supervised dimensionality reduction for various purposes. The *embedding*  $\phi : \mathbb{R}^p \rightarrow \mathbb{R}^m$  of a data point in  $\mathbf{x}$  is given simply by

$$\phi(\mathbf{x}) = (f_1(\mathbf{x}), \dots, f_m(\mathbf{x}))^\top. \quad (5)$$

We define the *path distance* between data points  $\mathbf{x}, \mathbf{x}' \in \mathbb{R}^p$  as the total absolute change in the target value in a line drawn between data points:

$$d_{path}(\mathbf{x}, \mathbf{x}') = \int_0^1 \left| \frac{\partial f(t\mathbf{x}' + (1-t)\mathbf{x})}{\partial t} \right| dt, \quad (6)$$

where the function  $f$  is defined in Eq. (1). We define the *embedding distance* between data points as Manhattan distance in the embedding space,

$$d_{emb}(\mathbf{x}, \mathbf{x}') = \sum_{j=1}^m |f_j(\mathbf{x}) - f_j(\mathbf{x}')|. \quad (7)$$

The embedding distance can be considered an upper bound for a path distance. The distances satisfy

$$|f(\mathbf{x}') - f(\mathbf{x})| \leq d_{path}(\mathbf{x}, \mathbf{x}') \leq d_{emb}(\mathbf{x}, \mathbf{x}'). \quad (8)$$

The lower bound of Eq. (8) is tight when  $f(t\mathbf{x}' + (1-t)\mathbf{x})$  is non-decreasing or non-increasing function in  $t \in [0, 1]$ . The upper bound is tight when, additionally,  $f_j(t\mathbf{x}' + (1-t)\mathbf{x})$  are for all  $j \in [m]$  non-decreasing (or all non-increasing) functions of  $t$ ; see Lemma 4 for a proof and Sect. F for visualizing the embedding space.

In the next section, we will experimentally demonstrate the usefulness of the above properties and provide some theoretical footing for them.

### 3.4 Computational Complexity

Solving the optimization problem of Eq. (3) takes  $O(npk)$  time, where  $k$  is the number of optimization iterations the LBFGS algorithm takes (we take  $k$  to be constant since, in practice, we restrict it to a reasonable value). The time complexity of the optimization process described in Sect. 3.2 is therefore  $O(npm)$ .

### 3.5 If There Is no Non-Linearity

If the model is linear, i.e.,  $g(z) = z$ , the optimization problem of Eq. (3) for  $f_1(\mathbf{x})$  reduces to OLS linear regression for regression with a quadratic loss function and to the standard logistic regression for classification with the logistic loss function; see Sect. A for a proof.

### 3.6 Relation to Other Boosting Algorithms

Almost all boosting algorithms have a model in the form of Eq. (1), consisting of  $m$  weak learners with high bias and low variance, which are trained sequentially (as in Sect. 3.2) to model the errors of subsequent modeling iterations. Typical choices for the loss function are, in addition to those mentioned in Sect. 3.1, exponential loss  $l_{exp}(y, y') = e^{-yy'}$  used by AdaBoost [7], and hinge loss  $l_{hinge}(y, y') = \max(0, 1 - yy')$  which can be thought of as non-smooth variant of the logistic loss. In many state-of-the-art algorithms, such as XGBOOST, the weak learner is often a tree-based classifier and not a perceptron-like entity of Eq. (2).

In principle, we could define embedding and the embedding distance similarly for any such boosting algorithm. Instead of tree-based approaches, GBMAP uses weak learners based on a simple perceptron structure to generate the embedding

coordinates, which provide new features via simple transformation of the original data, automatically ignoring non-relevant directions. These coordinates have the following desirable properties over the tree-based weak learners: the perceptrons provide smooth (not piece-wise constant) transformation of the covariate space; thus, neighboring points are not likely to overlap in the embedding. Due to the construction, the predicted target value increases or decreases linearly when we move outside the training data, with the slope being proportional to the importance of the direction to the supervised learning task, helping us to detect data points with potentially large prediction errors.

## 4 Numerical Experiments

### 4.1 Datasets and Algorithms

**Table 1.** Datasets used in the experiments.

DATASET	$n$	$p$	TARGET
ABALONE	4 177	8	$\mathbb{R}$
AIR QUALITY	7 355	11	$\mathbb{R}$
AUTOMPG	392	8	$\mathbb{R}$
CALIFORNIA	20 640	7	$\mathbb{R}$
CONCRETE	1 030	8	$\mathbb{R}$
CPU-SMALL	8 192	12	$\mathbb{R}$
QM9-10K	10 000	27	$\mathbb{R}$
SUPERCONDUCTOR	21 263	81	$\mathbb{R}$
SYNTH-COS-R	200 000	200	$\mathbb{R}$
WINE-RED	1 599	11	$\mathbb{R}$
WINE-WHITE	4 898	11	$\mathbb{R}$
BREAST-CANCER	569	30	$\pm 1$
DIABETES	768	8	$\pm 1$
EEG-EYE-STATE	14 980	14	$\pm 1$
GERMAN-CREDIT	1 000	20	$\pm 1$
HIGGS-10K	10 000	28	$\pm 1$
SYNTH-COS-C	200 000	200	$\pm 1$

We obtained ten real-world regression and five classification datasets shown in Tab. 1 from the UCI repository [17], OPENML [34], and SCIKIT-LEARN [25], described in more detail in Sect. C.

We additionally used a synthetic data SYNTH-COS-R( $n, p$ ) and SYNTH-COS-C( $n, p$ ) obtained as follows. We generated SYNTH-COS-R by first sampling the data matrix  $\mathbf{X} \in \mathbb{R}^{n \times p}$  from a Gaussian distribution with zero mean and unit variance and let  $\mathbf{y} = \alpha \cos(\mathbf{X})\mathbf{u}$ , where  $\cos(\mathbf{X}) \in \mathbb{R}^{n \times p}$  denotes element-wise  $\cos$ ,  $\alpha \in \mathbb{R}$ , and  $\mathbf{u} \in \mathbb{R}^p$  is a random unit vector. Finally, we center  $\mathbf{y}$  so that it has zero

means. We used  $\alpha = 5$  throughout this work. The classification dataset SYNTH-COS-C is obtained by passing the regression target values to the logistic function to obtain class probabilities (see Sect. A) and then randomly sampling the classification target values  $\{-1, +1\}$  based on these probabilities. The “default” values are  $n = 2 \cdot 10^5$  and  $p = 200$ , and we have also included the intercept term in  $\mathbf{X}$ .

The DRIFT datasets for Sect. 4.5 were obtained as follows. Given a real-world dataset, we split it into training and test datasets in a way that induces drift. We first find the most important feature to split the dataset that potentially produces drift. Specifically, for each feature, we split the data set into  $\mathbf{a}$  and  $\mathbf{b}$  of equal size according to the increasing order of that feature. We then further randomly split  $\mathbf{a}$  into  $\mathbf{a1}$ ,  $\mathbf{a2}$  where  $\mathbf{a1}$  and  $\mathbf{a2}$  are of roughly the same size. We then drop the chosen feature from all mentioned subsets and train a GBMAP regressor (or classifier) on  $\mathbf{a1}$  and compute the loss (squared loss if regression, logistic loss if classification) of its predictions on  $\mathbf{a2}$  and  $\mathbf{b}$ . By construction,  $\mathbf{a2}$  is assumed to come from the same distribution as the training data, while  $\mathbf{b}$  potentially has some drift in its distribution. We then use the difference between the loss on  $\mathbf{b}$  and the loss on  $\mathbf{a2}$  to measure how much drift the split induces and pick the feature that maximizes the drift.

We preprocessed all real-world datasets by subtracting the mean, dividing by standard deviation, one-hot encoding the categorical covariates, and adding the intercept terms (for GBMAP). We used OLS and logistic regression for the baseline comparisons in regression and classification tasks. We selected XGBOOST as the main comparison for both tasks. We chose the OLS and logistic regression implementations from SCIKIT-LEARN [25] and used XGBOOST from XGBOOST Python library [3].

We selected model hyperparameters by random search with 5-fold cross-validation (for OLS, no tuning is required). We gave the random search a budget of 100 iterations for each algorithm. For hyperparameter tuning, SYNTH-COS-R and SYNTH-COS-C were downsampled to  $n = 6 \cdot 10^4$ , and random search was given 10 iterations for efficiency. For logistic regression, we tuned only the  $L_2$ -penalty term. For XGBOOST, we selected the number of boosting iterations, max tree depth and subsampling rate for hyperparameter tuning. Finally, for GBMAP, we selected  $m$ ,  $\beta$ ,  $\lambda$ , and the maximum iterations for LBFGS. The ranges or distributions for parameter values are specified in Tab. 2.

We also compared the GBMAP distance to Euclidean distance in the supervised learning setting. To this end, we applied  $k$ -Nearest Neighbors ( $k$ -NN) with Euclidean distance and GBMAP  $L_1$  distance ( $k = 10$  for both variants). We chose the GBMAP hyperparameters similarly as above by random search but used only 50 iterations, and  $m$  was sampled from  $[2, 50]$ . We downsampled the real-world datasets to  $n = 10^4$  and used SYNTH-COS-R( $10^4, 20$ ) and SYNTH-COS-C( $10^4, 20$ ) for computational reasons.

## 4.2 Scaling

We conducted an experimental evaluation of the runtime performance (Tab. 3) of GBMAP, comparing it with LOL, IVIS and PCA. The evaluation was performed on



**Table 2.** Hyperparameter ranges for LR (logistic regression, XGBOOST and GBMAP.  $U(\cdot)$  denotes an uniform distribution.

MODEL	PARAMETER	RANGE
LR	$L_2$ -PENALTY	$U(10^{-5}, 1)$
XGBOOST	N-BOOSTS	100–2000
XGBOOST	MAXDEPTH	1–5
XGBOOST	SUBSAMPLE	[0.5, 0.6, ..., 1]
GBMAP	$m$ (N-BOOSTS)	2–150
GBMAP	SOFTPLUS $\beta$	1–20
GBMAP	MAXITER	[200, 400]
GBMAP	$\lambda$	$U(0, 10^{-2})$

a computing cluster, on which each run was allocated two processors and 64GB of RAM. We generated synthetic using `SYNTHETIC-COS-C( $n, p$ )`, with varying parameters  $n$  and  $p$ . The algorithm runtimes were averaged over ten repeated runs. We set  $m = 2$  in GBMAP, and the number of embedding components was also set to 2 for all other methods. We set  $\lambda = 10^{-3}$ ,  $\beta = 1$  and `MAXITER` = 100 for GBMAP. For `IVIS`, we used the default number of epochs 1000 from the official implementation with an early stopping set to 5 epochs. GBMAP scales roughly as  $O(np)$  and is quite fast. On data dimensionality scaling GBMAP is roughly comparable to `LOL`. Meanwhile, `IVIS` scales poorly, taking an order of magnitude longer to run.

**Table 3.** Wall clock runtimes in seconds, averaged over ten runs. Lower values are better.

$n$	$p$	GBMAP	IVIS	LOL	PCA
$10^5$	100	5.8	276.8	1.7	0.9
$10^5$	200	4.5	270.1	3.1	1.5
$10^5$	400	7.8	331.0	6.5	3.1
$10^5$	800	22.5	499.5	17.6	8.5
$10^5$	1600	79.1	932.5	53.9	27.3
$10^5$	3200	204.2	1688.2	195.8	106.3
$10^5$	25	1.4	286.4	0.2	0.1
$5 \cdot 10^5$	25	14.3	1719.3	1.1	0.5
$10^6$	25	14.2	4710.6	2.3	0.9
$5 \cdot 10^6$	25	174.8	18223.8	11.2	4.9
$10^7$	25	204.9	26623.5	22.3	9.8

### 4.3 Regression and Classification

The regression and classification experiments’ results ( $R^2$  and accuracy) are in the first block of columns of Tab. 4. We see that GBMAP is roughly comparable to XGBOOST across all datasets when we use GBMAP directly as a regressor/classifier. If we use the embedding distance produced by GBMAP in Eq. (7) as the proposal distance for  $k$ -NN, it can improve the performance of  $k$ -NN (the second block of columns of Tab. 4). For “easier” datasets where almost all features are relevant,  $k$ -NN gives comparable results with the Euclidean and embedding distances of Eq. (7), however, for more realistic datasets where this is not the case (e.g., CALIFORNIA, CONCRETE, QM9-10K, SYNTH-COS-R, SYNT-COS-C) the embedding distance outperforms the Euclidean one. Indeed, if we added random features to any datasets, the advantage of  $k$ -NN with the embedding distance would become even more prominent.

**Table 4.** Regression results ( $R^2$ , top) and classification results (accuracy, bottom). Columns GBMAP, LINREG (OLS or logistic regression), and XGBOOST show the performance of the respective regression/classification algorithms. The column KNN shows the  $k$ -NN performance with Euclidean distance and column KNN-GBMAP with the embedding distance of Eq. (7). AUC of GBMAP and EUCLID drifters are shown on the right-hand columns. An AUC of 0.5 corresponds to random guessing. Higher values are better for all columns.

DATASET	GBMAP	LINREG	XGBOOST	KNN	KNN-GBMAP	AUC-GBMAP	AUC-EUCLID
ABALONE	<b>0.577</b>	0.526	0.535	0.517	<b>0.556</b>	0.95	<b>0.96</b>
AIRQUALITY	<b>0.922</b>	0.905	0.912	<b>0.914</b>	0.912	<b>0.98</b>	0.96
AUTOMPG	<b>0.863</b>	0.784	0.807	0.840	<b>0.855</b>	<b>0.94</b>	0.91
CALIFORNIA	0.755	0.602	<b>0.841</b>	0.689	<b>0.767</b>	<b>0.74</b>	0.64
CONCRETE	0.907	0.582	<b>0.917</b>	0.634	<b>0.871</b>	0.73	<b>0.81</b>
CPU-SMALL	0.974	0.713	<b>0.978</b>	0.945	<b>0.974</b>	<b>0.91</b>	0.84
QM9-10K	0.701	0.471	<b>0.707</b>	0.574	<b>0.689</b>	<b>0.96</b>	0.87
SUPERCONDUCTOR	0.874	0.730	<b>0.911</b>	0.852	<b>0.869</b>	<b>0.98</b>	0.97
SYNTH-COS-R	<b>0.452</b>	0.00	0.025	0.411	<b>0.748</b>	–	–
WINE-RED	<b>0.396</b>	0.358	0.395	0.292	<b>0.362</b>	<b>0.85</b>	0.77
WINE-WHITE	0.395	0.290	<b>0.432</b>	0.335	<b>0.363</b>	<b>0.95</b>	0.89
BREAST-CANCER	0.965	0.953	<b>0.971</b>	0.947	<b>0.982</b>	0.51	<b>0.59</b>
DIABETES	0.766	<b>0.775</b>	0.758	0.727	<b>0.784</b>	0.63	<b>0.75</b>
EEG-EYE-STATE	0.755	0.642	<b>0.944</b>	0.773	<b>0.801</b>	0.66	<b>0.74</b>
GERMAN-CREDIT	0.730	<b>0.767</b>	0.733	0.703	<b>0.713</b>	<b>0.65</b>	0.63
HIGGS-10K	0.681	0.639	<b>0.703</b>	0.615	<b>0.661</b>	<b>0.70</b>	0.67
SYNTH-COS-C	<b>0.583</b>	0.50	0.582	0.593	<b>0.698</b>	–	–

#### 4.4 Supervised Learning Features

We evaluated GBMAP embeddings similarly to [35] by measuring the generalization error of a supervised model trained on embeddings. As the supervised learning models, we selected OLS linear regression for regression tasks and logistic regression for classification to demonstrate that even simple linear models can perform competitively with good features. We used half of the data for training and the other half to estimate the generalization error. The generalization error ( $R^2$  or accuracy) was calculated over five repeated splits. We compared the GBMAP embeddings in a supervised learning setting to other supervised embedding methods such as LOL, IVIS, and unsupervised PCA. We applied LOL only for classification datasets, as the method assumes class-label target values.

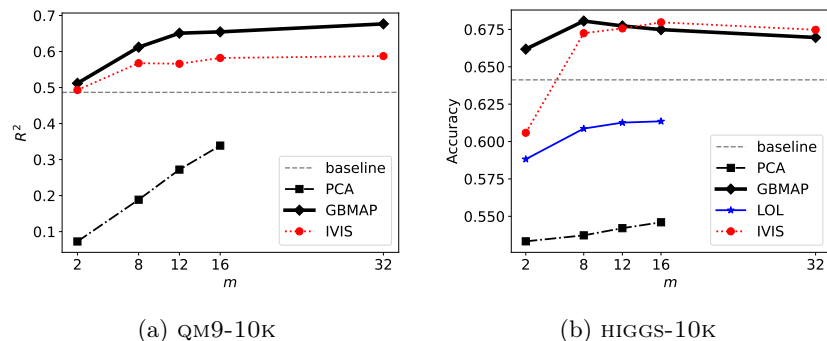
For IVIS, we set the maximum epochs to 1000 with early stopping set to 5 epochs, and we used mean absolute error as the supervision metric. We selected GBMAP  $\beta$  using random search with 10 iterations and set  $\lambda = 10^{-3}$  and maximum iterations for LBFGS optimizer  $\text{MAXITER} = 400$ . For the experiment, we selected datasets where the linear model compared poorly to more complex models (Sect. 4.3). We split the data randomly into half; one half was used to train the model and find the embedding, and the other was used to estimate generalization error. The above was repeated five times to control the randomness.

Fig. 1 presents the improved performance of linear regression and logistic regression when using new features extracted by various methods. The complete results for all datasets are in Sect. D. We can see that GBMAP provides good features for supervised learning, comparable to IVIS. On the other hand, LOL cannot improve the logistic regression at all. Likewise, as expected, PCA is merely a dimensionality reduction method; hence, its performance is worse than the baselines that use all original features.

Using GBMAP features, simple linear models can narrow the gap between complex and black-box models. Note that the GBMAP transformation is not restricted by the number of covariates  $p$ , unlike PCA and LOL.

#### 4.5 Out-of-Distribution Detection

In this subsection, we show how the embedding distance can be used to detect concept drift, i.e., when the test data follows a different distribution to the training data, resulting in deteriorating prediction performance. Following [23], we frame the drift detection problem as a binary classification problem; we say there is concept drift if a regression or classification loss on a new data point exceeds a pre-defined threshold. We introduce concept drift in real-world datasets using the splitting scheme described in Sect. 4.1, where we denote the training set by  $\mathbf{a1}$ , the in-distribution test set  $\mathbf{a2}$ , and the out-of-distribution set  $\mathbf{b}$ . We then train GBMAP on  $\mathbf{a1}$  and want to detect drift on the test datasets  $\mathbf{a2}$  and  $\mathbf{b}$ . We define a point as being out-of-distribution if the GBMAP error (squared loss if regression, logistic loss if classification) at that point is larger than a threshold here we use 95% quantile of the losses on  $\mathbf{a2}$ . For real-world applications, the threshold would be set by a domain expert.



**Fig. 1.** Embeddings as features for OLS regression (QM9-10K,  $R^2$ , (a)) and logistic regression (HIGGS-10K, accuracy, (b)). The baselines are OLS regression (a) and logistic regression (b) trained on the original data. The GBMAP transformation is not restricted by the data  $p$  (the number of covariates), unlike PCA and LOL and can be used to transform the data to arbitrary dimensions. The HIGGS-10K and QM9-10K has  $p < 32$  hence, the lines for PCA and LOL end at  $m = 16$ .

Our idea to detect drift is as follows. GBMAP and a  $k$ -NN model should give similar outputs within the training distribution. However, when moving outside the distribution, the GBMAP prediction increases or decreases linearly, with the slope depending on the importance of the direction to the supervised learning task. On the other hand, the  $k$ -NN prediction remains roughly constant when we move far outside the training data distribution. Therefore, we propose using the difference between the GBMAP and  $k$ -NN predictions as a drift indicator: if the prediction depends strongly on the prior modeling assumptions, we risk a larger-than-expected loss.

As the ground-truth loss, in regression, we use the squared difference between the actual target and the GBMAP prediction  $(y - f(x))^2$  and in classification, we use the squared difference between the actual score  $s$  and the GBMAP prediction. Here, by  $s$ , we refer to the values passed to the sigmoid to get class probabilities. In real-world datasets, as the actual score is unavailable, we use the score function estimated via logistic regression, i.e.,  $\hat{s}_i = \mathbf{w}^T \mathbf{x}_i$ , where we obtain the parameters  $\mathbf{w}$  by optimization over complete data  $\mathbf{w} = \arg \min_{\mathbf{w}} n^{-1} \sum_{i=1}^n \log(1 + e^{-y_i \hat{s}_i})$ .

Given a test point  $\mathbf{x}^*$ , we denote by  $\mathcal{N}(\mathbf{x}^*) \subseteq [n]$ , where  $|\mathcal{N}(\mathbf{x}^*)| = k$ , the  $k$  nearest training data points to  $\mathbf{x}^*$  using the distance produced by GBMAP embedding of Eq. (7). For regression, we use  $f_{kNN}(\mathbf{x}^*) = \sum_{i \in \mathcal{N}(\mathbf{x}^*)} y_i / k$ . For classification, the  $k$ -NN prediction of the score at  $\mathbf{x}^*$  is given by  $f_{kNN}(\mathbf{x}^*) = \sum_{i \in \mathcal{N}(\mathbf{x}^*)} f(\mathbf{x}_i) / k$ . The *drift indicator* for the GBMAP *drifter* is the difference between the GBMAP prediction at  $\mathbf{x}^*$  and this  $k$ -NN prediction, i.e.,  $|f(\mathbf{x}^*) - f_{kNN}(\mathbf{x}^*)|$ . By construction, the features irrelevant to the supervision tasks will likely be ignored by GBMAP and thus have little effect on the outcome.

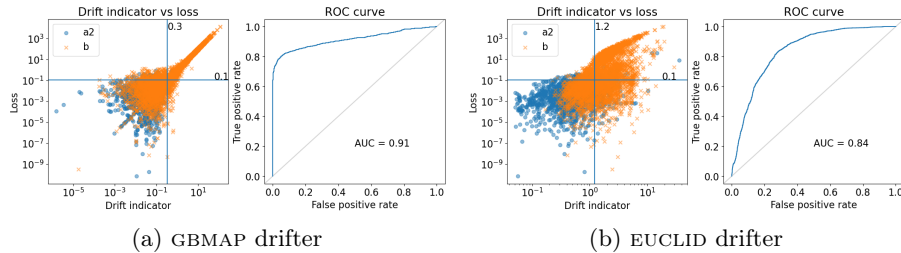


**Fig. 2.** The drift indicator against the loss figures (left) and ROC curves (right) for the GBMAP (left column) and EUCLID (right column) drifters on CPU-SMALL dataset. The horizontal line denotes our chosen concept drift threshold, while the vertical line indicates the drift indicator threshold that leads to maximal  $F_1$  score (not used in the analysis), as in [23]. The blue spheres are the data from the in-distribution set **a2**, and the orange crosses are the data from the out-of-distribution set **b**. The GBMAP drifter detects drift with a high AUC of 0.91, while the EUCLID has AUC of 0.84

As a baseline comparison, we use the Euclidean distance in the original data space from the test point  $\mathbf{x}^*$  to the  $k$ :th nearest training data point (EUCLID *drifter*). We chose  $k = 5$  for both drifters. We use the following parameters for GBMAP across all datasets: number of boosting steps  $m = 20$ , softplus  $\beta = 5$ , Ridge regularization  $\lambda = 10^{-3}$ , maximum number of the LBFSG optimizer iterations  $\text{MAXITER} = 200$ . We downsample the SUPERCONDUCTOR dataset for this drift experiment to  $n = 10^4$ .

Fig. 2 depicts the scatter plots between the error and the drift indicators as well as the Receiver Operating Characteristic (ROC) curves [5] of GBMAP and EUCLID drifters for the CPU-SMALL dataset. The GBMAP drift indicator is highly correlated with the error, as desired, superior to the Euclidean indicator. Figures for the other datasets are in Sect. E. The Area Under the Curve (AUC) values of the GBMAP and EUCLID drifters when detecting concept drift for regression and classification, respectively, are shown in the right-hand columns of Tab. 4. For the regression datasets, the GBMAP drifter is superior to the EUCLID drifter, while for classification datasets, both drifters perform similarly.

We note that for some datasets, the splitting scheme described in 4.1 fails to introduce any concept drift. This can happen when there are no clearly important covariates to the given supervised task, e.g., for CALIFORNIA only around 12% of the data points in the out-of-distribution set **b** have loss larger than the 95% quantile threshold, compared to the in-distribution set **a2**, which has by construction 5% of points labeled as drift. Also, the datasets DIABETES, GERMAN-CREDIT contain only slight drift and BREAST-CANCER contains no drift at all (the mean loss for **b** is lower than **a2**).

## 5 Other Uses for GBMAP

### 5.1 Supervision via Differences Between Models

The “default” choice is to have  $f_0(\mathbf{x}) = 0$ , but if we want for example, to study the errors made by a pre-trained supervised learning model  $h : \mathbb{R}^p \rightarrow \mathbb{R}$ , we can set  $f_0(\mathbf{x}) = h(\mathbf{x})$ , in which case the embedding tries to model the residuals of the model, effectively capturing the model’s shortcomings.

As a real-world example, consider a simple linear regression model  $h_1$  with a moderate  $R^2$  score and a black-box model (e.g., a deep neural network)  $h_2$  with a high  $R^2$  score. The challenge is to identify (semi)explainable features that can enhance the performance of the simple linear model, bringing it closer to the black-box model. In this case, we can set  $f_0 = h_1$  and treat the black-box model as the target function, i.e.,  $y_i = h_2(\mathbf{x}_i)$ . It is worth noting that the objective here is to interpret and find new features capturing the behavior of the black-box model, not the original data. The black-box model can provide labeled data for any region of interest, allowing us to create a (semi)white-box model that approximates the black-box model’s behavior in various regions, not just the training region. In another example, we can use GBMAP to find regions where these models exhibit the most significant differences. Of course, the absolute difference  $|h_1(\mathbf{x}) - h_2(\mathbf{x})|$  can be computed point-wise, but it does not give regions in a principled manner. We again turn to GBMAP, boosting from one model to another. By construction, GBMAP gives a sequence of hyperplanes  $\{\mathbf{x} \in \mathbb{R}^p \mid \mathbf{w}_j^T \mathbf{x} = 0\}$  that separate the feature space. Notably, the half-space activated by the softplus function indicates regions where the two models diverge, particularly in the initial GBMAP iterations. If a region is never activated, it suggests that the two models are likely similar in that specific region.

### 5.2 Explainability

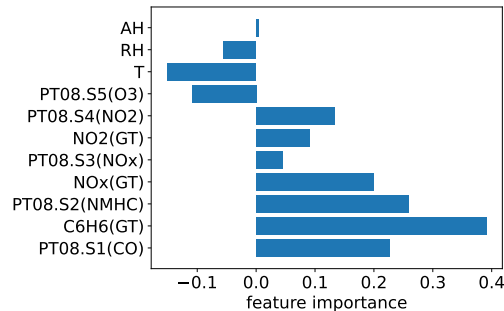


**Fig. 3.** Local feature importance in terms of local linear regression coefficients in the decision of GBMAP for the 50th training data point in the AIRQUALITY dataset. We have omitted the intercept term from the plot.

Unlike black-box models that require explainable AI (XAI) tools to give insight into why these models predict specific outcomes [10,1], our method is interpretable with its built-in XAI. The softplus-nonlinearity is a smooth approximation of the ReLU, which separates the feature space into two parts by a hyperplane and inactivates one part while letting another part be as-is. The feature space is therefore partitioned into several regions by each weak learner, and in each area, the GBMAP prediction is roughly piece-wise linear. Consequently, we can obtain the importance of each feature in that region and have local interpretable models for each decision in terms of the linear or logistic regression coefficients. For example, Fig. 3 shows the regression coefficients of each feature in the GBMAP prediction at the 50th training data point of the AIRQUALITY dataset. We can, from this figure, infer that **AH** plays no role in the prediction of GBMAP at this point, while **C6H6(GT)** is the most essential feature for this prediction. Recall that all features have been normalized to unit variance; hence, the regression coefficients can be interpreted directly as feature importance's.

## 6 Conclusion

We have proposed a novel supervised dimensional reduction method based on a boosting framework with simple perceptron-like weak learners. As a side-product, we obtain a competitive and interpretable supervised learning algorithm for regression and classification. The transformations defined by the boosting structure of weak learners can be used for feature creation or supervised dimensional reduction.

For finding features for regression or classification, we are at least as good as the competition, such as IVIS. Our advantage is the speed and more interpretable features obtained by a simple perception transformation. Indeed, if we drop the interpretability requirement, it would be trivial to make a good feature just by including the target variable predicted by a powerful black box regression/classification algorithm as one of the features! The GBMAP transformation induces a distance that ignores irrelevant directions in the data, which can be used to improve distance-based learning algorithms such as  $k$ -Nearest Neighbors. We also showed that GBMAP can reliably detect data points with potentially large prediction errors, which is important in practical applications, including concept drift.

Interesting future directions include a more in-depth study of GBMAP to detect concept drift and quantify the uncertainty of regressor/classifier predictions. Another interesting avenue for future work is visualization: how the found embedding and the embedding distance could also be used to make supervised embeddings of the data for visual inspection (initial example shown in Sect. F and Fig. 8).

**Acknowledgments.** We acknowledge the funding by the University of Helsinki and the Research Council of Finland (decisions 346376 and 345704).

**Disclosure of Interests.** The authors have no competing interests to declare relevant to the content of this article

## References

1. Björklund, A., Mäkelä, J., Puolamäki, K.: SLISEMAP: Combining Supervised Dimensionality Reduction with Local Explanations. In: Machine Learning and Knowledge Discovery in Databases, vol. 13718, pp. 612–616. Springer Nature Switzerland, Cham (2023). [https://doi.org/10.1007/978-3-031-26422-1\\_41](https://doi.org/10.1007/978-3-031-26422-1_41)
2. Blondel, M., Berthet, Q., Cuturi, M., Frostig, R., Hoyer, S., Llinares-López, F., Pedregosa, F., Vert, J.P.: Efficient and modular implicit differentiation. arXiv preprint arXiv:2105.15183 (2021)
3. Chen, T., Guestrin, C.: XGBoost: A Scalable Tree Boosting System. In: Proceedings of the 22nd ACM SIGKDD International Conference on Knowledge Discovery and Data Mining. pp. 785–794. ACM, San Francisco California USA (Aug 2016). <https://doi.org/10.1145/2939672.2939785>
4. De Vito, S., Massera, E., Piga, M., Martinotto, L., Di Francia, G.: On field calibration of an electronic nose for benzene estimation in an urban pollution monitoring scenario. *Sensors and Actuators B: Chemical* **129**(2), 750–757 (Feb 2008). <https://doi.org/10.1016/j.snb.2007.09.060>
5. Fawcett, T.: An introduction to ROC analysis. *Pattern Recognition Letters* **27**(8), 861–874 (2006). <https://doi.org/10.1016/j.patrec.2005.10.010>
6. Fernández-Delgado, M., Cernadas, E., Barro, S., Amorim, D.: Do we need hundreds of classifiers to solve real world classification problems? *Journal of Machine Learning Research* **15**(90), 3133–3181 (2014)
7. Freund, Y., Schapire, R.E.: A decision-theoretic generalization of on-line learning and an application to boosting. In: *Computational Learning Theory*, vol. 904, pp. 23–37. Springer Berlin Heidelberg, Berlin, Heidelberg (1995). [https://doi.org/10.1007/3-540-59119-2\\_166](https://doi.org/10.1007/3-540-59119-2_166)
8. Friedman, J.H.: Greedy function approximation: A gradient boosting machine. *The Annals of Statistics* **29**(5), 1189–1232 (2001). <https://doi.org/10.1214/aos/1013203451>
9. Gama, J., Žliobaitė, I., Bifet, A., Pechenizkiy, M., Bouchachia, A.: A survey on concept drift adaptation. *ACM Computing Surveys* **46**(4), 1–37 (2014). <https://doi.org/10.1145/2523813>
10. Guidotti, R., Monreale, A., Ruggieri, S., Turini, F., Giannotti, F., Pedreschi, D.: A Survey of Methods for Explaining Black Box Models. *ACM Computing Surveys* **51**(5), 1–42 (2019). <https://doi.org/10.1145/3236009>
11. Hamidieh, K.: Superconductivity Data (2018). <https://doi.org/10.24432/C53P47>
12. Hand, D.J.: Classifier Technology and the Illusion of Progress. *Statistical Science* **21**(1) (2006). <https://doi.org/10.1214/088342306000000060>
13. Hastie, T., Tibshirani, R., Friedman, J.H.: *The Elements of Statistical Learning: Data Mining, Inference, and Prediction*. Springer Series in Statistics, Springer, New York, NY, 2nd edn. (2009)
14. Hofmann, H.: Statlog (German Credit Data) (1994). <https://doi.org/10.24432/C5NC77>
15. I-Cheng Yeh: Concrete Compressive Strength (1998). <https://doi.org/10.24432/C5PK67>
16. Kahn, M.: Diabetes. <https://doi.org/10.24432/C5T59G>



17. Kelly, M., Longjohn, R., Nottingham, K.: The UCI Machine Learning Repository, <https://archive.ics.uci.edu>
18. Lindstrom, P., Mac Namee, B., Delany, S.J.: Drift detection using uncertainty distribution divergence. *Evolving Systems* **4**(1), 13–25 (2013). <https://doi.org/10.1007/s12530-012-9061-6>
19. Lu, J., Liu, A., Dong, F., Gu, F., Gama, J., Zhang, G.: Learning under Concept Drift: A Review. *IEEE Transactions on Knowledge and Data Engineering* pp. 1–1 (2018). <https://doi.org/10.1109/TKDE.2018.2876857>
20. van der Maaten, L., Hinton, G.: Visualizing Data using t-SNE. *Journal of Machine Learning Research* **9**(86), 2579–2605 (2008)
21. Matjaz Zwitter, M.S.: Breast Cancer (1988). <https://doi.org/10.24432/C51P4M>
22. Oikarinen, E., Puolamäki, K., Khoshrou, S., Pechenizkiy, M.: Supervised Human-Guided Data Exploration. In: *Machine Learning and Knowledge Discovery in Databases*, vol. 1167, pp. 85–101. Springer International Publishing, Cham (2020). [https://doi.org/10.1007/978-3-030-43823-4\\_8](https://doi.org/10.1007/978-3-030-43823-4_8)
23. Oikarinen, E., Tiittanen, H., Henelius, A., Puolamäki, K.: Detecting virtual concept drift of regressors without ground truth values. *Data Mining and Knowledge Discovery* **35**(3), 726–747 (May 2021). <https://doi.org/10.1007/s10618-021-00739-7>
24. Paulo Cortez, A.C.: Wine Quality (2009). <https://doi.org/10.24432/C56S3T>
25. Pedregosa, F., Varoquaux, G., Gramfort, A., Michel, V., Thirion, B., Grisel, O., Blondel, M., Prettenhofer, P., Weiss, R., Dubourg, V., Vanderplas, J., Passos, A., Cournapeau, D., Brucher, M., Perrot, M., Duchesnay, É.: Scikit-learn: Machine Learning in Python. *Journal of Machine Learning Research* **12**(85), 2825–2830 (2011)
26. Qahtan, A.A., Alharbi, B., Wang, S., Zhang, X.: A PCA-Based Change Detection Framework for Multidimensional Data Streams: Change Detection in Multidimensional Data Streams. In: *Proceedings of the 21th ACM SIGKDD International Conference on Knowledge Discovery and Data Mining*. pp. 935–944. KDD '15, Association for Computing Machinery, New York, NY, USA (Aug 2015). <https://doi.org/10.1145/2783258.2783359>
27. R. Quinlan: Auto MPG (1993). <https://doi.org/10.24432/C5859H>
28. Ramakrishnan, R., Dral, P.O., Rupp, M., von Lilienfeld, O.A.: Quantum chemistry structures and properties of 134 kilo molecules. *Scientific Data* **1**(1), 140022 (2014). <https://doi.org/10.1038/sdata.2014.22>
29. Revow, M.: Delve comp-activ dataset, <https://www.cs.toronto.edu/~delve/data/comp-activ/desc.html>
30. Roesler, O.: EEG Eye State (2013). <https://doi.org/10.24432/C57G7J>
31. Sethi, T.S., Kantardzic, M.: On the reliable detection of concept drift from streaming unlabeled data. *Expert Systems with Applications* **82**, 77–99 (2017). <https://doi.org/10.1016/j.eswa.2017.04.008>
32. Shao, J., Ahmadi, Z., Kramer, S.: Prototype-based learning on concept-drifting data streams. In: *Proceedings of the 20th ACM SIGKDD International Conference on Knowledge Discovery and Data Mining*. pp. 412–421. KDD '14, Association for Computing Machinery, New York, NY, USA (Aug 2014). <https://doi.org/10.1145/2623330.2623609>
33. Szubert, B., Cole, J.E., Monaco, C., Drozdov, I.: Structure-preserving visualisation of high dimensional single-cell datasets. *Scientific Reports* **9**(1), 8914 (2019). <https://doi.org/10.1038/s41598-019-45301-0>

34. Vanschoren, J., van Rijn, J.N., Bischl, B., Torgo, L.: Openml: Networked science in machine learning. *SIGKDD Explorations* **15**(2), 49–60 (2013). <https://doi.org/10.1145/2641190.2641198>
35. Vogelstein, J.T., Bridgeford, E.W., Tang, M., Zheng, D., Douville, C., Burns, R., Maggioni, M.: Supervised dimensionality reduction for big data. *Nature Communications* **12**(1), 2872 (2021). <https://doi.org/10.1038/s41467-021-23102-2>
36. Warwick Nash, T.S.: Abalone (1994). <https://doi.org/10.24432/C55C7W>
37. Whiteson, D.: HIGGS (2014)
38. Wold, S., Esbensen, K., Geladi, P.: Principal component analysis. *Chemometrics and Intelligent Laboratory Systems* **2**(1), 37–52 (1987). [https://doi.org/10.1016/0169-7439\(87\)80084-9](https://doi.org/10.1016/0169-7439(87)80084-9)
39. Žliobaitė, I., Pechenizkiy, M., Gama, J.: An Overview of Concept Drift Applications. In: *Big Data Analysis: New Algorithms for a New Society*, vol. 16, pp. 91–114. Springer International Publishing, Cham (2016). [https://doi.org/10.1007/978-3-319-26989-4\\_4](https://doi.org/10.1007/978-3-319-26989-4_4)

**Appendix.** The main text is self-contained and can be read and understood without the following appendix. Here, we present proofs and derivations for completeness. We also have included some complementary experimental results that we decided to exclude from the main text for compactness and lack of space.

## A GBMAP Reduces to OLS Linear and Logistic Regression if There Is no Non-Linearity

In this section, we study the case where  $f_0(\mathbf{x}) = 0$  and there is no non-linearity, i.e.,  $g(z) = z$ . We show that in that case, GBMAP reduces to OLS linear regression and logistic regression, both with Ridge regularization, and that after the first boosting iteration ( $j \geq 2$ ), the coefficients are of the order of  $O(\lambda)$ . Non-linearity is, therefore, essential to have non-trivial solutions with more than one embedding coordinate. We state this formally with the following Lemma.

**Lemma 1.** *The optimization problem for  $f_1$  ( $j = 1$ ) of Eq. (3) reduces for ordinary least squares linear regression with  $b_1 = 1$  for the quadratic loss and standard logistic regression for the logistic loss, both with Ridge regularization, if there is no nonlinearity, i.e.,  $g(z) = z$ . The parameters of subsequent weak learners  $f_j$  for  $j \geq 2$  are proportional to  $a_j = O(\lambda^{j-1})$  and  $\mathbf{w}_j = (O(\lambda^{j-1}), \dots, O(\lambda^{j-1}))^\top$  and they vanish in the absence of the regularization term (i.e., if  $\lambda = 0$ ).*

*Proof. Regression.* For the regression problem and quadratic loss  $l_{quadratic}(y, y') = (y - y')^2$ , the optimization problem of Eq. (3) reduces to

$$a_1, b_1, \mathbf{w}_1 = \arg \min_{a_1, b_1, \mathbf{w}_1} \left( n^{-1} \sum_{i=1}^n (y_i - a_1 - b_1 \mathbf{w}_1^\top \mathbf{x}_i)^2 + \lambda \|\mathbf{w}_1\|_2^2 \right) \quad (9)$$

We can, without loss of generality, take  $b_1 = 1$ , because changing  $\mathbf{w}_1 \leftarrow b_1 \mathbf{w}_1$  and  $b_1 \leftarrow 1$  leaves the loss unchanged.

Eq. (9) defines OLS linear regression with Ridge regularization. In the absence of regularization ( $\lambda = 0$ ), OLS linear regression gives the unbiased estimator, for which reason  $a_j = 0$  and  $\mathbf{w}_j = (0, \dots, 0)^\top$  for  $j \geq 2$ . However, in the presence of regularization, we have  $a_j = O(\lambda)$  and  $\mathbf{w}_j = (O(\lambda), \dots, O(\lambda))^\top$  for  $j \geq 2$  due to the fact that Ridge regression provides a biased estimator. The subsequent terms ( $j > 2$ ) are proportional to  $O(\lambda^{j-1})$ , respectively.

**Classification.** The “standard” logistic regression is a generalized linear model using the logit link function and maximum likelihood loss for the binomial distribution.

The probability that  $y = +1$  given  $\mathbf{x}$  is then given by  $p(y = +1 | \mathbf{x}) = \sigma(\mathbf{w}^\top \mathbf{x})$  and a probability of  $y = -1$  by  $p(y = -1 | \mathbf{x}) = 1 - \sigma(\mathbf{w}^\top \mathbf{x})$ , where  $\sigma(z) = 1/(1+e^{-z})$  is the sigmoid function or the inverse of the logit link function.

The log-loss for observation  $(\mathbf{x}, y)$  is then given by

$$\begin{aligned}
L &= -I(y = +1) \log p(y = +1 | \mathbf{x}) - I(y = -1) \log p(y = -1 | \mathbf{x}) \\
&= -I(y = +1) \log (\sigma(\mathbf{w}^\top \mathbf{x})) - I(y = -1) \log (1 - \sigma(\mathbf{w}^\top \mathbf{x})) \\
&= -I(y = +1) \log (\sigma(\mathbf{w}^\top \mathbf{x})) - I(y = -1) \log (\sigma(-\mathbf{w}^\top \mathbf{x})) \\
&= -I(y = +1) \log (\sigma(y\mathbf{w}^\top \mathbf{x})) - I(y = -1) \log (\sigma(y\mathbf{w}^\top \mathbf{x})) \\
&= -(I(y = +1) + I(y = -1)) \log (\sigma(y\mathbf{w}^\top \mathbf{x})) \\
&= -\log (\sigma(y\mathbf{w}^\top \mathbf{x})) \\
&= \log \left( 1 + e^{-y\mathbf{w}^\top \mathbf{x}} \right) = l_{\text{logistic}}(y, \mathbf{w}^\top \mathbf{x}),
\end{aligned} \tag{10}$$

where we have used  $\sigma(z) = 1 - \sigma(-z)$  and  $l_{\text{logistic}}(y, y') = \log \left( 1 + e^{-yy'} \right)$ .

For the classification problem, the optimization problem of Eq. (3) reduces to

$$a_1, b_1, \mathbf{w}_1 = \arg \min_{a_1, b_1, \mathbf{w}_1} \left( n^{-1} \sum_{i=1}^n l_{\text{logistic}}(y_i, a_1 + b_1 \mathbf{w}_1^\top \mathbf{x}_i) + \lambda \|\mathbf{w}_1\|_2^2 \right). \tag{11}$$

We can, without loss of generality, take  $b_1 = 1$ , because changing  $\mathbf{w}_1 \leftarrow b_1 \mathbf{w}_1$  and  $b_1 \leftarrow 1$  leaves the loss unchanged.

Eq. (11) defines the standard logistic regression with logit link function and Binomial loss with Ridge regularization. In the absence of regularization ( $\lambda = 0$ ), the logistic regression gives the unbiased estimator, for which reason  $a_j = 0$  and  $\mathbf{w}_j = (0, \dots, 0)^\top$  for  $j \geq 2$ . However, in the presence of regularization, we have  $a_j = O(\lambda)$  and  $\mathbf{w}_j = (O(\lambda), \dots, O(\lambda))^\top$  for  $j \geq 2$  because Ridge regression provides a biased estimator.

As described in the proof above, in classification tasks with logistic loss, the predicted probability of +1 is given by  $\hat{p}(y = +1 | \mathbf{x}) = \sigma(f(\mathbf{x}))$ , and the value of the response given the probability of one is given by as  $f(\mathbf{x}) = \sigma^{-1}(\hat{p}(y = +1 | \mathbf{x}))$ , where the sigmoid function is given by  $\sigma(z) = 1/(1 + e^{-z})$  and the logit function by  $\sigma^{-1}(p) = \log(p/(1 - p))$ . We can, therefore, use the logit function to transform outputs of a probabilistic classifier, outputting class probabilities, to the GBMAP response space  $y$ , if necessary, and the sigmoid function to obtain class probabilities from the response space.

## B Properties of the Distance Measures

We define in Eq. (7) the *embedding distance* and in Eq. (6) *path distance*. Here, we show the intuition behind the distances and prove the inequality of Eq. (8).

The “default” distance between points  $\mathbf{x} \in \mathbb{R}^p$  and  $\mathbf{x}' \in \mathbb{R}^p$  is given by the Euclidean distance  $\|\mathbf{x} - \mathbf{x}'\|_2$  or the Manhattan distance  $\|\mathbf{x} - \mathbf{x}'\|_1$ . However, these distances have the undesirable property that they weigh all directions equally, including those irrelevant to the supervised learning task. For this reason, we have defined a path distance in Eq. (6). The path distance between  $\mathbf{x}$  and  $\mathbf{x}'$  is the total absolute change of the function  $f$  when traversing a straight line  $t\mathbf{x}' + (1-t)\mathbf{x}$  from  $\mathbf{x}$  to  $\mathbf{x}'$ , parameterized by  $t \in [0, 1]$ . Next, we show some useful properties of the integral.

**Lemma 2.** *If  $f(t\mathbf{x}' + (1-t)\mathbf{x})$  is non-decreasing or non-increasing function in  $t \in [a, b]$  for some  $a < b$  then*

$$\int_a^b \left| \frac{\partial f(t\mathbf{x}' + (1-t)\mathbf{x})}{\partial t} \right| dt = |f(\mathbf{x}_a) - f(\mathbf{x}_b)|, \quad (12)$$

where  $\mathbf{x}_a = a\mathbf{x}' + (1-a)\mathbf{x}$  and  $\mathbf{x}_b = b\mathbf{x}' + (1-b)\mathbf{x}$ .

*Proof.* If  $f(t\mathbf{x}' + (1-t)\mathbf{x})$  is non-decreasing, its derivative is non-negative, we can drop  $|\square|$ , and the integral is simply

$$\begin{aligned} \int_a^b \left| \frac{\partial f(t\mathbf{x}' + (1-t)\mathbf{x})}{\partial t} \right| dt &= \int_a^b \frac{\partial f(t\mathbf{x}' + (1-t)\mathbf{x})}{\partial t} dt \\ &= f(\mathbf{x}_b) - f(\mathbf{x}_a) \\ &= |f(\mathbf{x}_a) - f(\mathbf{x}_b)|, \end{aligned} \quad (13)$$

where the second equality follows from the definition of the integral and the last from the fact that the function is non-decreasing, i.e.,  $f(\mathbf{x}_b) \geq f(\mathbf{x}_a)$ . We get the same expression if  $f(t\mathbf{x}' + (1-t)\mathbf{x})$  is non-increasing function in  $t \in [a, b]$ , i.e., the gradient is negative and  $f(\mathbf{x}_a) \geq f(\mathbf{x}_b)$ :

$$\begin{aligned} \int_a^b \left| \frac{\partial f(t\mathbf{x}' + (1-t)\mathbf{x})}{\partial t} \right| dt &= - \int_a^b \frac{\partial f(t\mathbf{x}' + (1-t)\mathbf{x})}{\partial t} dt \\ &= f(\mathbf{x}_a) - f(\mathbf{x}_b) \\ &= |f(\mathbf{x}_a) - f(\mathbf{x}_b)|. \end{aligned} \quad (14)$$

We have the following lemma for functions that are neither decreasing nor increasing.

**Lemma 3.** *Assume we can still split the axis  $t \in [0, 1]$  into  $k$  segments, where  $t_0 = 0 \leq t_1 \leq \dots \leq t_{k-1} \leq t_k = 1$  such that  $f(t\mathbf{x}' + (1-t)\mathbf{x})$  is either non-decreasing or non-increasing function in each of the  $k$  intervals  $t \in [t_{l-1}, t_l]$  for all  $l \in [k]$ . The path distance can be expressed as a sum of absolute changes of the residual function:*

$$d_{path}(\mathbf{x}, \mathbf{x}') = \sum_{l=1}^k |f(t_{l-1}\mathbf{x}' + (1-t_{l-1})\mathbf{x}) - f(t_l\mathbf{x}' + (1-t_l)\mathbf{x})|. \quad (15)$$

*Proof.* The proof follows directly from Lemma 2.

The Lemma below proves Eq. (8).

**Lemma 4.** *The path and embedding distances of Eqs. (6) and (7) satisfy the bounds of Eq. (8), i.e.,*

$$|f(\mathbf{x}') - f(\mathbf{x})| \leq d_{path}(\mathbf{x}, \mathbf{x}') \leq d_{emb}(\mathbf{x}, \mathbf{x}').$$

*Proof.* The sum of Eq. (15) is lower-bounded by  $|f(\mathbf{x}') - f(\mathbf{x})|$ , because of the triangle inequality  $|a - c| \leq |a - b| + |b - c|$  for any  $a, b, c \in \mathbb{R}$ . According to Lemma 2, the lower bound is tight when  $f(t\mathbf{x}' + (1 - t)\mathbf{x})$  is increasing or decreasing function in  $t \in [0, 1]$ .

We can rewrite the path distance as

$$\begin{aligned} d_{path}(\mathbf{x}, \mathbf{x}') &= \int_0^1 \left| \frac{\partial f(t\mathbf{x}' + (1 - t)\mathbf{x})}{\partial t} \right| dt \\ &= \int_0^1 \left| \sum_{j=1}^m \frac{\partial f_j(t\mathbf{x}' + (1 - t)\mathbf{x})}{\partial t} \right| dt \\ &\leq \sum_{j=1}^m \int_0^1 \left| \frac{\partial f_j(t\mathbf{x}' + (1 - t)\mathbf{x})}{\partial t} \right| dt \\ &= \sum_{j=1}^m |f_j(\mathbf{x}') - f_j(\mathbf{x})| \\ &= d_{emb}(\mathbf{x}, \mathbf{x}'), \end{aligned} \tag{16}$$

where we have used the definition of the function  $f$  in Eq. (1) for the second equality and  $\left| \sum_j a_j \right| \leq \sum_j |a_j|$  for any  $a_j \in \mathbb{R}$  for the inequality. The second last equality follows from the Lemma 2 and the fact that each of the  $f_j(t\mathbf{x}' + (1 - t)\mathbf{x})$  is as a softplus function either an increasing or decreasing function in  $t$ , resulting in the upper bound in Eq. (8).

## C Real-World Datasets

The following datasets in Tab. 1 are from the UCI repository [17]:

- AUTOMPG The target here is to predict the fuel consumption of cars using their physical properties [27].
- ABALONE The aim here is to predict the age of the Abalone snails using their physical properties [36].
- WINE-RED Is a red wine subset of the Wine Quality dataset containing various physicochemical properties of wines [24].
- WINE-WHITE Corresponding white wine subset of Wine Quality dataset.
- CONCRETE The objective here is to predict the compressive strength of concrete samples based on their physical and chemical properties [15].
- AIR-QUALITY Contains hourly averaged air quality measurements spanning approximately one year [4].
- DIABETES The aim here is to classify the occurrence of diabetes based on diagnostic measurements [16].
- GERMAN-CREDIT The objective here is to classify people as having good or bad credit risk based on attributes like employment duration, credit history, and loan purpose [14].
- BREAST-CANCER The goal is to classify breast cancer tumors as malignant or benign based on features derived from biopsy samples [21].

The following datasets in Tab. 1 are from the OPENML [34]:

- CPU-SMALL The aim here is to predict the system activity of a CPU [29].
- HIGGS-10K A subset HIGGS dataset [37] used for classifying particle processes as signal or background noise.
- EEG-EYE-STATE The target in this dataset is to determine the eye state (open or closed) based on EEG brainwave data [30].
- QM9-10K A subset of 10 000 heavies molecules from qm9 dataset [28].
- SUPERCONDUCTOR Contains information about chemical properties of superconductors [11].

The following dataset in Tab. 1 was loaded from SCIKIT-LEARN [25]:

- CALIFORNIA The goal here is to predict the price of houses in California, USA, using geographical characteristics and construction.

## **D Supervised Learning Features Results**

Tab. 5 presents supplementary results to Sect. 3.3.



**Table 5.** Feature creation experiment results. Top:  $R^2$ , bottom: accuracy, standard deviation on parenthesis. Higher values are better. Note that IVIS crashed on multiple occasions on the datasets with many data points, and LOL requires classification labels. Results are missing for PCA and LOL when  $p < m$  as it is not possible to select more components  $m$  than the data covariates  $p$

DATASET	$m$	GBMAP	PCA	IVIS	LOL
CALIFORNIA	2	0.64 ( $\pm$ 0.01)	0.03 ( $\pm$ 0.01)	<b>0.72</b> ( $\pm$ <b>0.01</b> )	–
CALIFORNIA	8	0.72 ( $\pm$ 0.01)	0.61 ( $\pm$ 0.01)	<b>0.77</b> ( $\pm$ <b>0.01</b> )	–
CALIFORNIA	12	0.73 ( $\pm$ 0.01)	$p < m$	<b>0.77</b> ( $\pm$ <b>0.01</b> )	–
CALIFORNIA	16	0.73 ( $\pm$ 0.01)	$p < m$	<b>0.77</b> ( $\pm$ <b>0.01</b> )	–
CALIFORNIA	32	0.74 ( $\pm$ 0.01)	$p < m$	<b>0.78</b> ( $\pm$ <b>0.01</b> )	–
CONCRETE	2	<b>0.73</b> ( $\pm$ <b>0.04</b> )	0.11 ( $\pm$ 0.06)	CRASH	–
CONCRETE	8	<b>0.85</b> ( $\pm$ <b>0.01</b> )	0.62 ( $\pm$ 0.03)	0.76 ( $\pm$ 0.03)	–
CONCRETE	12	<b>0.85</b> ( $\pm$ <b>0.02</b> )	$p < m$	0.78 ( $\pm$ 0.03)	–
CONCRETE	16	<b>0.86</b> ( $\pm$ <b>0.02</b> )	$p < m$	0.78 ( $\pm$ 0.04)	–
CONCRETE	32	<b>0.85</b> ( $\pm$ <b>0.05</b> )	$p < m$	0.78 ( $\pm$ 0.03)	–
CPU-SMALL	2	<b>0.97</b> ( $\pm$ <b>0</b> )	0.36 ( $\pm$ 0.02)	0.94 ( $\pm$ 0.02)	–
CPU-SMALL	8	<b>0.97</b> ( $\pm$ <b>0</b> )	0.69 ( $\pm$ 0.01)	<b>0.97</b> ( $\pm$ <b>0</b> )	–
CPU-SMALL	12	<b>0.97</b> ( $\pm$ <b>0</b> )	0.72 ( $\pm$ 0.01)	<b>0.97</b> ( $\pm$ <b>0</b> )	–
CPU-SMALL	16	<b>0.97</b> ( $\pm$ <b>0.01</b> )	$p < m$	<b>0.97</b> ( $\pm$ <b>0</b> )	–
CPU-SMALL	32	<b>0.97</b> ( $\pm$ <b>0.01</b> )	$p < m$	<b>0.97</b> ( $\pm$ <b>0</b> )	–
SUPERCONDUCTOR	2	0.82 ( $\pm$ 0)	0.46 ( $\pm$ 0.01)	<b>0.83</b> ( $\pm$ <b>0.01</b> )	–
SUPERCONDUCTOR	8	0.84 ( $\pm$ 0)	0.56 ( $\pm$ 0)	<b>0.85</b> ( $\pm$ <b>0.01</b> )	–
SUPERCONDUCTOR	12	0.84 ( $\pm$ 0.01)	0.59 ( $\pm$ 0)	<b>0.85</b> ( $\pm$ <b>0.01</b> )	–
SUPERCONDUCTOR	16	0.84 ( $\pm$ 0)	0.60 ( $\pm$ 0)	<b>0.86</b> ( $\pm$ <b>0.01</b> )	–
SUPERCONDUCTOR	32	<b>0.85</b> ( $\pm$ <b>0</b> )	0.69 ( $\pm$ 0.01)	<b>0.85</b> ( $\pm$ <b>0.01</b> )	–
QM9-10K	2	<b>0.51</b> ( $\pm$ <b>0.01</b> )	0.07 ( $\pm$ 0)	0.49 ( $\pm$ 0.09)	–
QM9-10K	8	<b>0.61</b> ( $\pm$ <b>0.02</b> )	0.19 ( $\pm$ 0.01)	0.57 ( $\pm$ 0.04)	–
QM9-10K	12	<b>0.65</b> ( $\pm$ <b>0.02</b> )	0.27 ( $\pm$ 0.01)	0.57 ( $\pm$ 0.03)	–
QM9-10K	16	<b>0.66</b> ( $\pm$ <b>0.02</b> )	0.34 ( $\pm$ 0.01)	0.58 ( $\pm$ 0.03)	–
QM9-10K	32	<b>0.68</b> ( $\pm$ <b>0.02</b> )	$p < m$	0.59 ( $\pm$ 0.03)	–
SYNTH-COS-R	2	<b>0.06</b> ( $\pm$ <b>0</b> )	0 ( $\pm$ 0)	CRASH	–
SYNTH-COS-R	8	<b>0.16</b> ( $\pm$ <b>0</b> )	0 ( $\pm$ 0)	CRASH	–
SYNTH-COS-R	12	<b>0.20</b> ( $\pm$ <b>0</b> )	0 ( $\pm$ 0)	CRASH	–
SYNTH-COS-R	16	0.23 ( $\pm$ 0)	0 ( $\pm$ 0)	<b>0.64</b> ( $\pm$ <b>0.01</b> )	–
SYNTH-COS-R	32	<b>0.34</b> ( $\pm$ <b>0</b> )	0 ( $\pm$ 0)	CRASH	–
SYNTH-COS-R	64	0.46 ( $\pm$ 0)	0 ( $\pm$ 0)	<b>0.66</b> ( $\pm$ <b>0.01</b> )	–
SYNTH-COS-R	128	<b>0.52</b> ( $\pm$ <b>0</b> )	0 ( $\pm$ 0)	CRASH	–
HIGGS-10K	2	<b>0.66</b> ( $\pm$ <b>0.01</b> )	0.53 ( $\pm$ 0.01)	0.61 ( $\pm$ 0.02)	0.59 ( $\pm$ 0.01)
HIGGS-10K	8	<b>0.68</b> ( $\pm$ <b>0.01</b> )	0.54 ( $\pm$ 0.01)	0.67 ( $\pm$ 0.01)	0.61 ( $\pm$ 0.01)
HIGGS-10K	12	<b>0.68</b> ( $\pm$ <b>0.01</b> )	0.54 ( $\pm$ 0)	<b>0.68</b> ( $\pm$ <b>0.01</b> )	0.61 ( $\pm$ 0.01)
HIGGS-10K	16	<b>0.68</b> ( $\pm$ <b>0.01</b> )	0.55 ( $\pm$ 0)	<b>0.68</b> ( $\pm$ <b>0.01</b> )	0.61 ( $\pm$ 0.01)
HIGGS-10K	32	0.67 ( $\pm$ 0.01)	$p < m$	<b>0.68</b> ( $\pm$ <b>0.01</b> )	$p < m$
EEG-EYE-STATE	2	<b>0.61</b> ( $\pm$ <b>0.01</b> )	0.55 ( $\pm$ 0)	0.60 ( $\pm$ 0.01)	0.57 ( $\pm$ 0)
EEG-EYE-STATE	8	0.65 ( $\pm$ 0.01)	0.57 ( $\pm$ 0.01)	<b>0.80</b> ( $\pm$ <b>0.01</b> )	0.58 ( $\pm$ 0.01)
EEG-EYE-STATE	12	0.69 ( $\pm$ 0.02)	0.62 ( $\pm$ 0.01)	<b>0.80</b> ( $\pm$ <b>0.01</b> )	0.61 ( $\pm$ 0.01)
EEG-EYE-STATE	16	0.71 ( $\pm$ 0.01)	$p < m$	<b>0.81</b> ( $\pm$ <b>0.01</b> )	$p < m$
EEG-EYE-STATE	32	0.75 ( $\pm$ 0.01)	$p < m$	<b>0.81</b> ( $\pm$ <b>0.01</b> )	$p < m$
SYNTH-COS-C	2	<b>0.56</b> ( $\pm$ <b>0</b> )	0.50 ( $\pm$ 0)	CRASH	0.50 ( $\pm$ 0)
SYNTH-COS-C	8	<b>0.59</b> ( $\pm$ <b>0</b> )	0.50 ( $\pm$ 0)	CRASH	0.50 ( $\pm$ 0)
SYNTH-COS-C	12	<b>0.60</b> ( $\pm$ <b>0</b> )	0.50 ( $\pm$ 0)	CRASH	0.50 ( $\pm$ 0)
SYNTH-COS-C	16	0.61 ( $\pm$ 0)	0.50 ( $\pm$ 0)	<b>0.67</b> ( $\pm$ <b>0</b> )	0.50 ( $\pm$ 0)
SYNTH-COS-C	32	<b>0.62</b> ( $\pm$ <b>0</b> )	0.50 ( $\pm$ 0)	CRASH	0.50 ( $\pm$ 0)
SYNTH-COS-C	64	0.64 ( $\pm$ 0)	0.50 ( $\pm$ 0)	<b>0.68</b> ( $\pm$ <b>0</b> )	0.50 ( $\pm$ 0)
SYNTH-COS-C	128	<b>0.64</b> ( $\pm$ <b>0</b> )	0.50 ( $\pm$ 0)	CRASH	0.50 ( $\pm$ 0)

## E Out-of-Distribution Detection

### E.1 Regression Datasets

Fig. 4 and Fig. 5 show the results of the GBMAP and the EUCLID drifters on all considered regression datasets. There is a clear correlation between the GBMAP drift indicator and the actual loss, explaining the high AUC values (around 0.9 for most datasets) reported in Tab. 4 (the last block of columns). Meanwhile, the EUCLID indicator is inferior for most datasets.

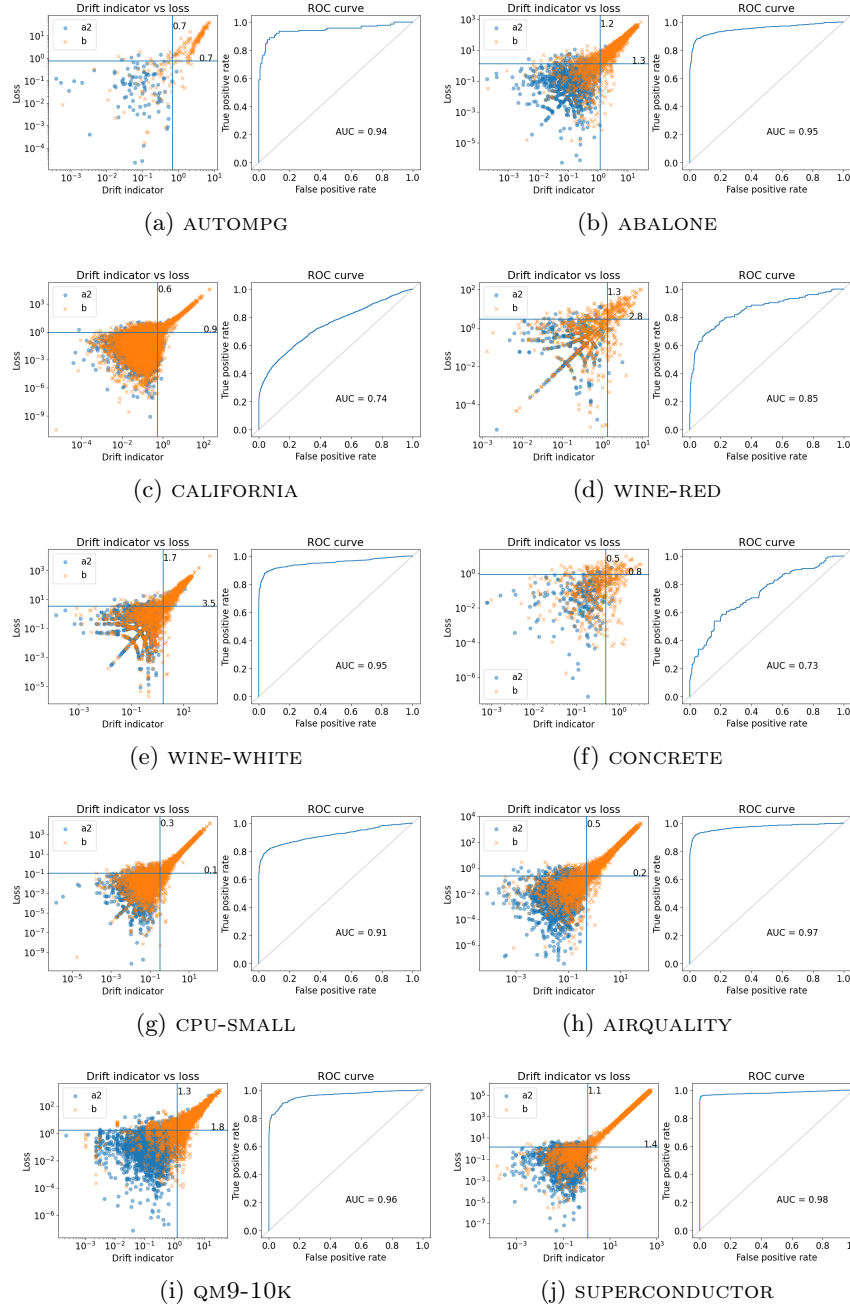


Fig. 4. GBMAP drifter for regression datasets

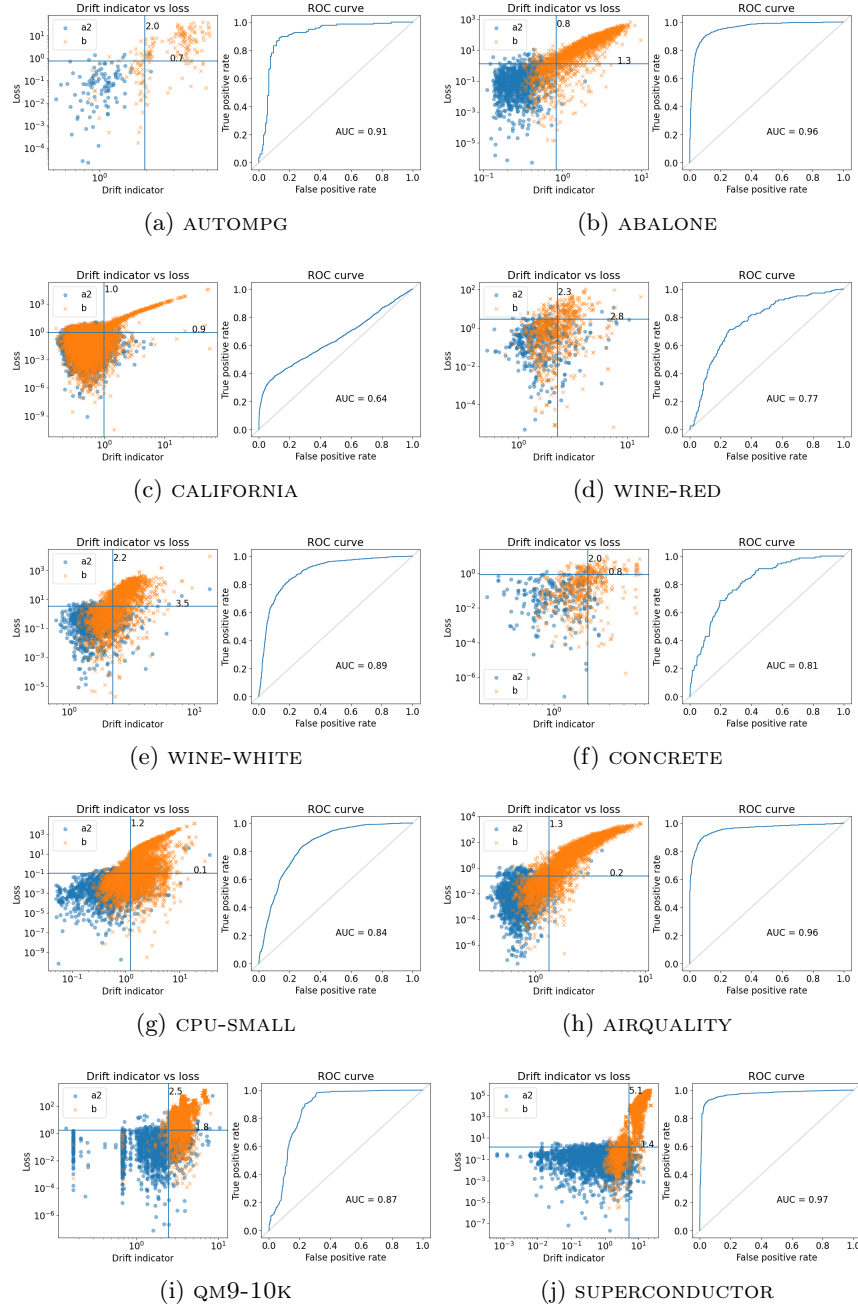


Fig. 5. EUCLID drifter for regression datasets

E.2 Classification Datasets

Fig. 6 and Fig. 7 show the results of the GBMAP drifter and the EUCLID drifter on all considered classification datasets. The drifters perform similarly for the classification datasets.

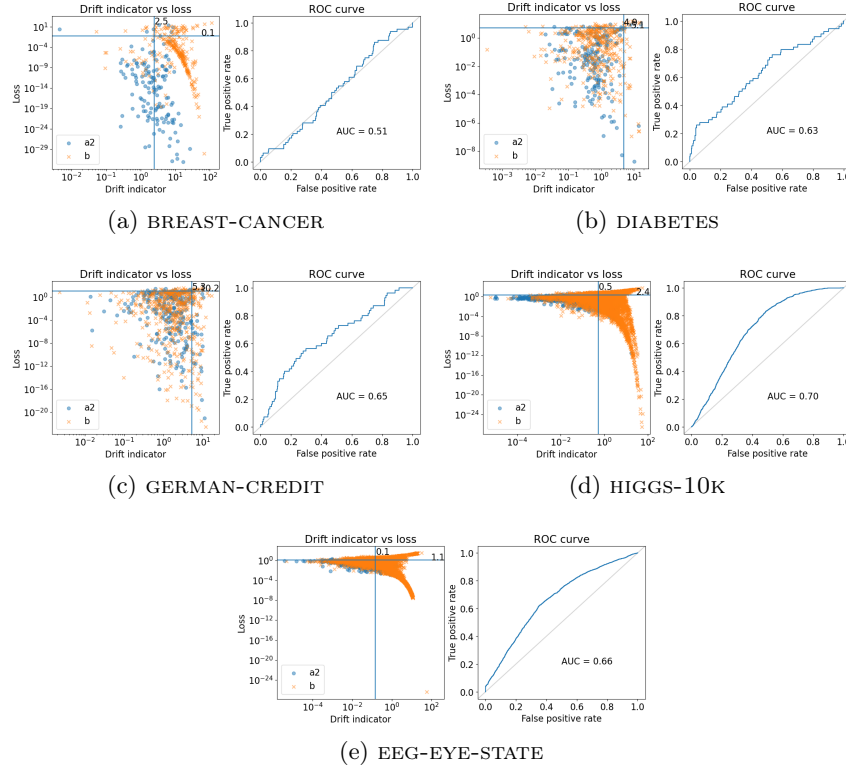
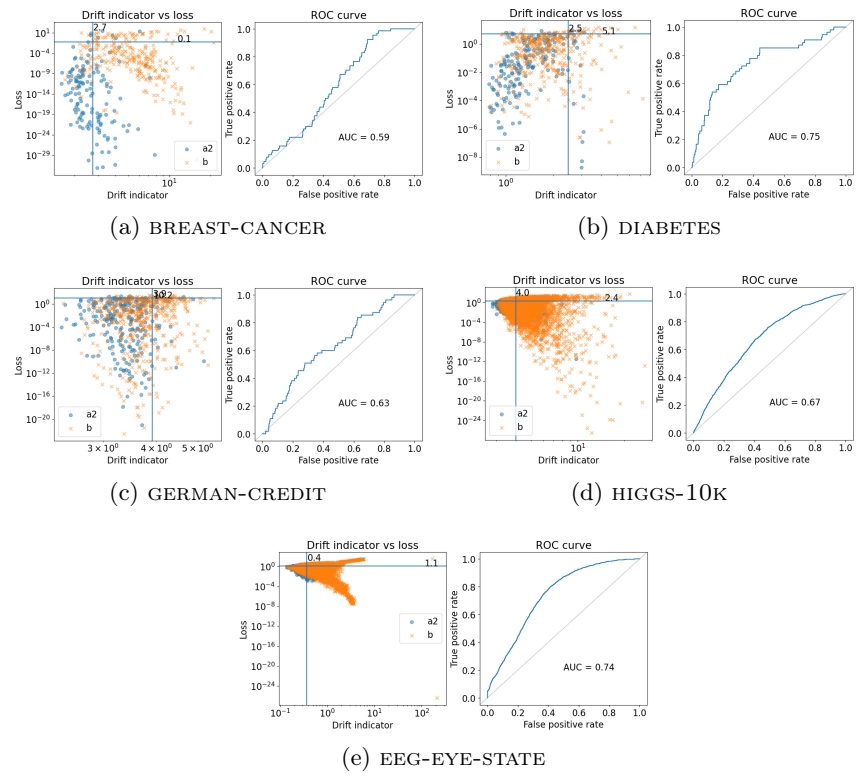
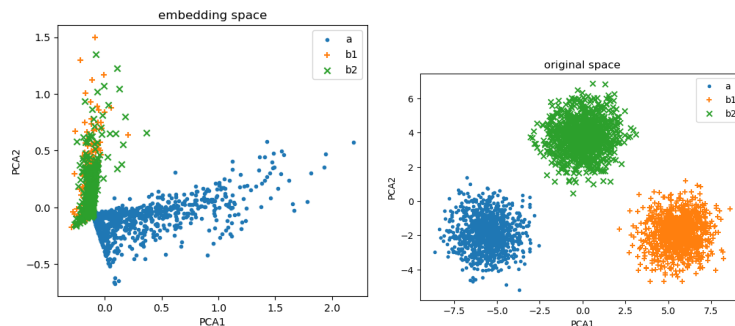


Fig. 6. GBMAP drifter for classification datasets



**Fig. 7.** EUCLID drifter for classification datasets

## F Visualizations



**Fig. 8.** PCA of the embedding (left) and the original space (right).

Here, we show an example of a visualization of the embedding space by PCA and compare it to the PCA visualization of the original data space, demonstrating some properties of the embedding and the embedding distance.

Consider an 8-dimensional (plus the intercept term) synthetic regression dataset, similar to SYNTH-COS-R, where there are three equal-sized clusters (**a**, **b1**, **b2**) in the covariate space and where dimensions 1–4 are relevant for the regression task, and dimensions 5–8 are irrelevant for the regression task. Further, assume that the cluster **a** differs from cluster **b2** in the relevant dimensions 1–4 and the cluster **b1** differs from **b2** only in the irrelevant dimensions 5–8. We expect an unsupervised dimensionality reduction method, such as PCA, to show three clusters. However, if the PCA is done on the embedding space, clusters **b1** and **b2** should merge since their difference is irrelevant for the regression task and the irrelevant directions should be ignored by the embedding, which is what happens; see the visualization in Fig. 8.

Specifically, the data matrix  $\mathbf{X} \in \mathbb{R}^{3000 \times 9}$  is constructed as follows, where  $\mathbf{N}_{ij}$  are independent draws from a normal distribution with zero mean and unit variance:

$$\mathbf{X}_{ij} = \begin{cases} \mathbf{N}_{ij} + 4, & i \in \{1, \dots, 1000\} \wedge j \in \{1, 2, 3, 4\} \\ \mathbf{N}_{ij} + 4, & i \in \{1001, \dots, 2000\} \wedge j \in \{5, 6, 7, 8\} \\ 1, & j = 9 \\ \mathbf{N}_{ij}, & \text{otherwise} \end{cases} \quad (17)$$

The regression target vector  $\mathbf{y} \in \mathbb{R}^{3000}$  is given by

$$\mathbf{y} = \cos(\mathbf{X})\mathbf{u}, \quad (18)$$

where  $\mathbf{u} \in \mathbb{R}^9$  is a random unit vector satisfying  $\mathbf{u}_5 = \mathbf{u}_6 = \mathbf{u}_7 = \mathbf{u}_8 = \mathbf{u}_9 = 0$  and  $\cos(\cdot)$  denotes element-wise cosine.

Cluster **a** is composed of points  $\mathbf{X}_i$  where  $i \in \{1, \dots, 1000\}$ , cluster **b1** is composed of points  $\mathbf{X}_i$  where  $i \in \{1001, \dots, 2000\}$ , and cluster **b2** is composed of points  $\mathbf{X}_i$  where  $i \in \{2001, \dots, 3000\}$ .

We have used the parameters  $m = 10$ ,  $\lambda = 10^{-3}$ , and  $\beta = 5$  for GBMAP.